

# Device Selection for the Coexistence of URLLC and Distributed Learning Services

Milad Ganjalizadeh<sup>\*†</sup>, Hossein S. Ghadikolaei<sup>\*</sup>, Deniz Gündüz<sup>‡</sup>, and Marina Petrova<sup>†§</sup>

<sup>\*</sup>Ericsson Research, Sweden

<sup>†</sup>School of Electrical Engineering and Computer Science, KTH Royal Institute of Technology, Stockholm, Sweden

<sup>‡</sup>Department of Electrical and Electronic Engineering, Imperial College London, London, UK

<sup>§</sup>Mobile Communications and Computing, RWTH Aachen University, Germany

Email: {milad.ganjalizadeh, hossein.shokri.ghadikolaei}@ericsson.com, d.gunduz@imperial.ac.uk, petrovam@kth.se

**Abstract**—Recent advances in distributed artificial intelligence (AI) have led to tremendous breakthroughs in various communication services, from fault-tolerant factory automation to smart cities. When distributed learning is run over a set of wirelessly connected devices, random channel fluctuations and the incumbent services running on the same network impact the performance of both distributed learning and the coexisting service. In this paper, we investigate a mixed service scenario where distributed AI workflow and ultra-reliable low latency communication (URLLC) services run concurrently over a network. Consequently, we propose a risk sensitivity-based formulation for device selection to minimize the AI training delays during its convergence period while ensuring that the operational requirements of the URLLC service are met. To address this challenging coexistence problem, we transform it into a deep reinforcement learning problem and address it via a framework based on soft actor-critic algorithm. We evaluate our solution with a realistic and 3GPP-compliant simulator for factory automation use cases. Our simulation results confirm that our solution can significantly decrease the training delay of the distributed AI service while keeping the URLLC availability above its required threshold and close to the scenario where URLLC solely consumes all network resources.

**Index Terms**—6G, availability, distributed AI, factory automation, federated learning, reinforcement learning, SGD, URLLC.

## I. INTRODUCTION

Future 6G networks are envisioned as an unprecedented evolution from connected things to connected intelligence, thereby serving as the backbone of a cyber-physical world with the integration of connected devices, intelligence, and humans [1]. Numerous 6G artificial intelligence (AI) applications have emerged recently to improve efficiency and system performance in many vertical sectors, such as industrial automation [2], autonomous driving [3], and enhanced mobile broadband [4]. Promising performance gains of AI models come with the significant training workload relying on the massive amount of data collected by the edge devices. Centralized training of the models can be impractical in many wireless communication applications because of i) the distributed nature of the data

generated/collected by mobile devices, ii) privacy concerns of sharing the local data with a central server, especially when the computational server is managed by a third party operator, and iii) limited wireless resources (in terms of bandwidth and power). Therefore, privacy-preserving distributed AI techniques have become the cornerstone of recent advancements in AI applications over wireless networks. In most distributed training algorithms, a set of devices upload their local updates (e.g., local gradients in distributed gradient descent (DGD) [5], or local model updates in federated learning (FL) [6]) via an uplink (UL) channel to a central node (or a set of nodes) that maintains global parameters and orchestrates the iterations of the distributed training algorithm. Once the central node updates the global model, it shares it with the devices over a downlink (DL) channel for the next iteration.

To highlight the complex interplay between the AI workflow and the underlying communication services, we note that the performance of distributed learning algorithms is affected by the errors and random delays in UL/DL transmissions as well as the AI parameters (e.g., model size, data quality, and training algorithm) [7]–[9]. More specifically, the wall-clock convergence time of distributed training algorithms depend on i) the time delay of every iteration (e.g., the amount of time in which global model parameters are transmitted to the devices, trained locally, and transmitted back to the central node), and ii) the number of iterations. The former is not only a function of the model and data sizes, but also the quality of the wireless channel between the central node and individual computational devices. The general perception is that increasing the AI model size improves the training accuracy [10], given enough data samples and a proper training approach that reduces over-fitting. However, using a larger AI model also means longer communication and computation time, resulting in a potentially higher convergence time [7], [11]. Higher AI communication overheads may also be detrimental for other communication services running in parallel to the AI. The tighter the requirements of the underlying service, the harder to design smooth coexistence.

Ultra-reliable low-latency communications (URLLC) is characterized by strict requirements in terms of latency, which could be as short as 500  $\mu$ s, and availability, which could be as high as 99.999999 [12]. In [12], [13], 3rd Generation Partnership Project (3GPP) defines *communication service*

This work has been submitted to the IEEE for possible publication. Copyright may be transferred without notice, after which this version may no longer be accessible.

This work was supported by Swedish Foundation for Strategic Research (SSF) under Grant iPhD:ID17-0079.

*availability* as the mean proportion of time during which the communication service meets the required quality of service (QoS) of the application it serves. Regarded as the most challenging use case in 5G and beyond 5G, this type of service is supposed to enable challenging applications (e.g., factory automation or autonomous intelligent transport systems [14]) that have not been feasible in preceding generations of wireless communication systems.

#### A. Uniqueness of Coexistence of URLLC and Distributed AI

There exist a rich literature when it comes to conventional mixed services between URLLC and enhanced mobile broadband (e.g., [15], [16]), URLLC and massive machine type communication (e.g., [17]), or even all three together (e.g., [18]). Notice that there are two main fundamental differences between distributed AI services and other traditional communication traffic. First, the performance of these conventional services is characterized by the statistics of a communication metric (e.g., throughput or energy consumption for enhanced mobile broadband and massive machine type communication, respectively). Nevertheless, distributed training service is an iterative and collaborative task aiming to solve an optimization problem as quickly as possible. Hence, the performance may not be affected only by the transmission characteristics of a single device. The potential statistical correlation of data of various devices allows distributed learning to operate using a carefully chosen subset of devices. Moreover, higher quality updates from few devices at each iteration may be more beneficial than lower quality updates from many devices [19], showing that sum throughput is not the right metric due to the dependence among data across different devices. Second, in addition to well-known decision parameters for other communication services, distributed AI has a unique set of decision variables such as the model size, choice of algorithm, and selection of devices participating in the training task. However, to the best of our knowledge, no literature exists on the coexistence of distributed AI and URLLC services in which both communication and learning aspects are jointly considered. Despite the lack of such analysis, numerous 6G AI applications have emerged recently to improve efficiency and system performance in various cyber-physical control applications such as industrial automation [2], and autonomous driving [20]. We believe the adoption and success of such applications depend highly on the analysis and optimization of these scenarios with existing URLLC services, which serves as the main motivation of our work.

#### B. Distributed AI over Wireless Networks

The main challenges of running distributed training over wireless networks arise from its two main characteristics: i) the dynamics of wireless propagation, which depends on various factors in the network, such as noise, interference, and fading, and ii) resource (e.g., bandwidth and transmit power) scarcity [8]. The latter becomes even more significant since distributed training requires many iterations exchanging typically large models or model parameters [8]. From the communication service perspective, several recent studies have focused on

resource management and device selection techniques. References [19], [21]–[24] leverage resource management and, more explicitly, device selection to improve the performance of distributed learning in terms of training loss or convergence time. For example, in [23], the authors evaluated the effects of resource management, device selection, and transmit power on FL convergence and optimized these wireless parameters to reduce FL training loss. Reference [24] proposes an FL algorithm that can handle heterogeneous user data assuming strong convex and smooth loss functions. The resource allocation is then optimized to improve the convergence of the proposed algorithm. In [19], it is shown that the performance of distributed learning can be improved if the device selection algorithm jointly considers the updates from the devices with their channel conditions. Nevertheless, none of these works address the mixed service scenario where the distributed learning performance is determined not only by the wireless network characteristics and limitations but also by the demands on the higher priority service.

#### C. Contributions:

As distinct services, the performance of both URLLC and distributed AI over wireless networks have been widely investigated in the existing literature. However, the coexistence of URLLC, with its stringent requirements, and distributed AI workflow, with its unique traffic model and performance characteristics, have not yet been discussed in the literature. Such coexistence introduces new fundamental challenges as well as unique trade-offs between URLLC latency and availability on the one hand, and convergence time and accuracy of distributed AI on the other hand. When running the distributed AI training over some clusters, under ideal processing and communications assumptions, increasing the model size and/or the number of participating AI devices at each iteration will often lead to better convergence. However, when distributed learning is run over a set of wireless devices, because of interference and limited available bandwidth, various parameters (e.g., signal to noise and interference ratio (SINR), packet error ratio, and queuing delays) might impact the training delay to the extent that the improvement in convergence rate may become nonessential. When URLLC comes into the picture, the performance becomes bounded by two more factors, i.e., competing with higher priority traffic and URLLC availability requirements. The latter is use case specific and, depending on the requirements' strictness and the use case sensitivity these requirements, increasing the model size and/or the number of participating AI devices can have a non-linear detrimental effect on the distributed AI performance.

In this paper, we focus on the understanding and optimizing the coexistence of distributed learning and URLLC services. We introduce a soft synchronous distributed learning protocol in which the central node broadcasts the global model updates upon receiving local updates from a subset of the available devices. Then, leveraging deep reinforcement learning (DRL), we develop a framework to dynamically select a set of participating AI devices in order to minimize the convergence time of the distributed learning task while maintaining the

strict URLLC availability requirements. *To the best of our knowledge, this is the first work that comprehensively studies and optimizes the underlying trade-offs between the URLLC performance and the distributed AI workflow, simultaneously running on the same wireless network.* In summary, our contributions are as follows:

- We develop a model for the operational metrics of the URLLC service (i.e., communication service availability) and essential parameters that characterize AI training workflow (i.e., training delay, model size, convergence, and accuracy) and investigate the interplay between them. Since the system is resource-limited (in terms of bandwidth and transmission power) and URLLC availability requirements are strict, a subset of devices must be selected to perform each iteration of distributed AI. Accordingly, we formulate an optimization problem that minimizes the average training latency of the distributed AI to reach  $\epsilon$ -accuracy while sustaining URLLC’s communication service availability requirements.
- We transform the formulated coexistence optimization problem into a Markov decision process (MDP) and design an action masking technique to put a lower bound on the minimum number of AI devices required to participate in each iteration of distributed training. However, the solution may select a higher number of devices than this minimum to address the so-called *straggling effect*.
- To deal with the unknown dynamics of our complex cellular system, we propose a data-driven approach that optimizes the device selection policy via a state-of-the-art off-policy DRL algorithm, namely soft actor-critic (SAC). In our scheme, the device selection policy of each AI device is distributed across distinct neurons, resulting in a linear increase in the SAC output size with the number of devices.
- We evaluate our framework utilizing a 3GPP-compliant 5G simulator in a factory automation use case. We observe that the number of participating AI devices can significantly impact the performance of URLLC. Our results provides important insights for the ongoing standardization activities of distributed AI.

The rest of this paper is organized as follows. We provide the necessary preliminaries on the distributed learning, and our system model in Section II and Section III, respectively. We then formulate the problem in Section IV. Section V presents the proposed MDP modeling and DRL-based device selection. We describe our simulation methodology in Section VI, and discuss the results in Section VII. Finally, Section VIII concludes the paper.

*Notations:* Normal font  $x$  or  $X$ , bold font  $\mathbf{x}$ , bold font  $\mathbf{X}$ , and uppercase calligraphic font  $\mathcal{X}$  denote scalars, vectors, matrices and sets, respectively. We denote by  $[X]$  the set  $\{1, 2, \dots, X\}$ , by  $[\mathbf{x}]_i$  element  $i$  of vector  $\mathbf{x}$ , by  $[\mathbf{X}]_{i,j}$  the element  $ij$  of matrix  $\mathbf{X}$ , and by  $|\mathcal{X}|$  the cardinality of set  $\mathcal{X}$ . We define  $\mathbb{1}\{\mathbf{x}\}$  as the element-wise indicator function returning  $\mathbf{y}$ , where  $[\mathbf{y}]_i$  takes 1 when condition  $[\mathbf{x}]_i$  holds, and 0, otherwise. The curled inequality ( $\geq$  or  $>$ ) represents element-wise inequality. We use  $\mathbf{1}$  and  $\mathbf{0}$  to denote all-one

and all-zero vectors, respectively.

## II. BACKGROUND ON DISTRIBUTED LEARNING

Consider the problem of minimizing a sum of smooth functions  $\{f_i : \mathbb{R}^d \mapsto \mathbb{R}\}_{i \in [N]}$ , with corresponding gradients  $\{\nabla f_i : \mathbb{R}^d \mapsto \mathbb{R}^d\}_{i \in [N]}$ :

$$\mathbf{w}^* := \min_{\mathbf{w} \in \mathbb{R}^d} f(\mathbf{w}) = \min_{\mathbf{w} \in \mathbb{R}^d} \frac{1}{N} \sum_{i \in [N]} f_i(\mathbf{w}). \quad (1)$$

Such problems frequently arise in distributed learning where  $N$  is the number of distributed devices,  $f$  could express the global loss function, and each  $f_i$  could represent a local loss function. In practice, to parallel the computations or to preserve the privacy of local datasets, we use distributed algorithms to solve (1) [25]. That is, at iteration  $k$ , a subset of the workers compute and upload their local gradients  $\{\nabla f_i(\mathbf{w}_k)\}_i$  to a central node, which updates the model and broadcasts the updated model parameters  $\mathbf{w}_{k+1}$  back to the workers.<sup>1</sup> FL is another popular method in which the workers will run one or several local training passes before uploading their local models. The central node will then take a global average over them. The communication overhead is almost the same as uploading gradients [3]. However, most of these UL messages (gradients or local models) may be redundant, carrying almost no additional information since they can be retrieved from their past communicated messages as well as messages of other devices [27]. Forcing some of them to remain silent would i) reduce UL interference to other users, ii) increase throughput, and iii) improve latency.

In conventional synchronous distributed training methods, the central node waits until it receives the local updates from all participating devices, leading to a considerable inactive time at the central node as well as faster devices waiting for stragglers. To tackle the straggling problem, in  $n$ -sync approaches, the central node only waits for a subset of participating devices, say  $n$  out of all  $N$  devices, and updates the global model using their messages at every iteration [5]. Nevertheless, vanilla  $n$ -sync-based methods add extra load on the underlying communication system, as they will ask all the devices to upload their data, and the central node starts its update with the first  $n$  received data. Reference [28] proposed an algorithm to adjust  $n$  at every iteration. References [6], [27], [29] proposed various approaches to eliminate some unnecessary uploads. However, none of those works study or optimize the interplay between distributed learning and other parallel communication services.

## III. SYSTEM MODEL

### A. Network Model

We consider an industrial automation scenario, where a set of  $\mathcal{G} := [G]$  gNodeBs (gNBs), each consisting of 1 cell, serve a set of  $\mathcal{U} := [U]$  industrial devices in the factory hall execute different functions that enable automated production.

<sup>1</sup>We have a similar set of trade-offs and solutions for non-smooth functions, where we cannot define gradients. The major difference compared to this paper is that instead of updating based on gradients, we may need to update based on its generalizations, like subgradients [26].

The communication system should timely and reliably deliver i) monitoring data to gNBs and ii) computed or emergency control commands to the actuators.

For simplicity, we assume that the AI devices are distinct from the industrial devices, and there exist a set of  $\mathcal{N}:=|N|$  AI devices. Moreover, we assume that the AI central node needs to receive the relevant local information from  $n$  out of these  $N$  AI devices to update its global model at each iteration. To tackle the straggler effect, the AI central node might request an update from  $\mathcal{N}_{m,k} \subseteq \mathcal{N}$  at iteration  $k$ , where  $|\mathcal{N}_{m,k}|=m_k (\geq n)$  of the devices to participate in the training. Hence, at  $k$ th iteration, the central node might request  $m_k - n$  extra backup devices to mitigate the straggler problem in a synchronous distributed learning scenario.

To manage the coexistence of two services, where the priority of services are inherently different, 5G and beyond 5G envision two approaches. The first approach, employed in this paper, is to use the existing standardized protocols in 5G-NR for QoS handling. In this case, each connected device is assigned with one or several QoS flows and data radio bearers, where the former is set in the core network, depending on the service QoS requirements. For example, in our scenario, the traffic from/to URLLC devices is set to have high priority QoS flow to ensure low latency, whilst the traffic from/to AI devices is set to have low priority QoS flow. Each (or several) of these QoS flows are then mapped to a data radio bearer in the radio access network (RAN). In gNB and devices, there is an associated radio link control (RLC) buffer to each data radio bearer, and in our case, with strict priority scheduling [30]. The second approach is to have separate slices for URLLC and distributed AI, resulting in full resource separation (e.g., in terms of bandwidth).

### B. Distributed Learning Process

We consider a network of  $N$  AI devices that cooperatively solve a distributed learning problem. Assuming that  $\mathcal{N}_{n,k} \subseteq \mathcal{N}_{m,k}$  is the subset of size  $n$  whose updates the central node receives first at iteration  $k$ , then iteration  $k$  of an abstract distributed algorithm reads:

$$\mathbf{w}_{k+1} = A(\mathbf{c}_{i,k}, \mathbf{w}_k), \quad \text{for } \forall i \in \mathcal{N}_{n,k} \quad (2a)$$

$$\mathbf{c}_{i,k} = C_i(\mathbf{w}_k), \quad \text{for } \forall i \in \mathcal{N}_{m,k} \quad (2b)$$

where function  $A$  represents an algorithm update of the decision variable  $\mathbf{w}_k$ , function  $C_i$  picks out the relevant information,  $\mathbf{c}_{i,k}$ , that node  $i$  uploads to the server to run the algorithm. This general algorithmic framework covers many machine learning algorithms, including FL and DGD, with or without data compression. For example, when  $C_i$  returns a stochastic gradient, say  $\tilde{\nabla} f_i(\mathbf{w}_k)$ , and  $A = \mathbf{w}_k - \eta \sum_i \tilde{\nabla} f_i(\mathbf{w}_k) / n$  for some positive step size  $\eta$ , we recover  $n$ -sync and synchronous DGD for  $n(<N)$  and  $n(=N)$  [5], respectively. When  $C_i$  returns an updated local model parameters of AI device  $i$  and  $A$  takes an averaging step over a subset of  $n(\leq N)$  AI devices, we recover FL ( $n$ -sync or synchronous). Without loss of generality, and for the sake of simplicity, we assume that the gradients' noise are independent and identically distributed [31].

### C. Channel Model

To model the channel, we consider a multiple-input and multiple-output system in which we leverage the time varying 3D spatial channel model from 3GPP in [32]. In this model, channels are characterized via clustering the multipath components, arriving at antenna arrays, in delay and double-directional angle (i.e., the zenith and azimuth of the angle-of-arrivals at the receiver and angle-of-departures at the transmitter). For simplicity, let us assume that  $N_g$  and  $N_d$  are respectively the number of antenna elements of gNB and devices. We denoted by  $\mathbf{H}_{x,y}(\tau; t) \in \mathbb{C}^{N_d \times N_g}$  the baseband channel response at time  $t$  to an input impulse at time  $t - \tau$ , between  $x$ th device and  $y$ th gNB in DL. Then, an entry of  $\mathbf{H}_{x,y}(\tau; t)$  for  $p$ th receiving antenna element and  $q$ th transmitting antenna element can be computed as

$$[\mathbf{H}_{x,y}(\tau; t)]_{p,q} := \sum_{l=1}^{N_c} \sqrt{\beta_l^{x,y}} \sum_{s=1}^{N_s} (\mathbf{g}_p^{x,y}(t, l, s))^T \mathbf{F}_{\text{xp}}^{x,y}(t, l, s) \mathbf{g}_q^{x,y}(t, l, s) e^{j\Upsilon_{p,q}^{x,y}(t, l, s)} \delta(\tau - \tau_{p,l,s}), \quad (3)$$

where  $N_c$  and  $N_s$  are respectively the number of clusters and rays, and  $\beta_l^{x,y}$  is a function of path loss, shadowing and  $l$ th cluster normalized power. Besides,  $\mathbf{g}_p^{x,y}(\cdot)$  is the field patterns of  $p$ th receiving element that  $s$ th ray of  $l$ th cluster has in the direction defined by arriving zenith and azimuth angles,  $\mathbf{F}_{\text{xp}}^{x,y}(\cdot)$  is  $2 \times 2$  matrix modeling the cross polarization power ratio for  $s$ th ray of  $l$ th cluster,  $\mathbf{g}_q^{x,y}(\cdot)$  is the field patterns of  $q$ th transmitting element that  $s$ th ray of  $l$ th cluster has in the direction defined by departing zenith and azimuth angles,  $\Upsilon_{p,q}^{x,y}(\cdot)$  is a function of location vector of  $p$ th receiving and  $q$ th transmitting element as well as the Doppler frequency, and finally,  $\tau_{p,l,s}$  is the propagation delay of  $s$ th ray in  $l$ th cluster. For UL,  $\mathbf{H}_{x,y}(\tau; t)$  can be derived by swapping  $p$  and  $q$  in (3).

Note that although we leverage the 3GPP statistical spatial channel model [32], our problem formulation (Section IV-C) and solution approach (Section V) are general and not limited to this channel model. In the next section, we use these models to formulate our performance metrics.

## IV. PERFORMANCE METRICS AND PROBLEM FORMULATION

### A. URLLC Metric: Communication Service Availability

The players in operational, information and communication technologies are entering new territory in which 5G is utilized to connect industries. The main challenge in such a merger is ensuring that the operational requirements are fulfilled during a 5G system's operating phase [33]. One well-accepted metric in the operational technology domain is availability. Hence, 3GPP, as the primary standardization consortium for mobile telecommunications, has attempted to specify the requirements for communication service availability from the application layer perspective in [12], [13]. The main difference between the end-to-end communication service performance and the observed performance on the network layer is driven by a system parameter called *survival time*,  $T_{\text{sv}}$ . Survival time is the duration of time for which the application layer can tolerate

failures in the communication system without any performance degradation in availability [34]. We denote the network layer state by a Bernoulli random variable  $X_i^\Gamma(t)$ , where  $\Gamma \in \{\text{UL}, \text{DL}\}$ , and  $X_i^\Gamma(t)$  for the  $i$ th URLLC device is zero if the last packet is not received at the communication interface within a specified delay bound, because either it could not be decoded at the lower layers or faced excessive retransmission, and/or queuing delays. Consequently, assuming that application recovery time is negligible, we define the per-device application layer state variable,  $Y_i^\Gamma(t)$  as

$$Y_i^\Gamma(t) := \begin{cases} 0, & \text{if } \int_{t-T_{sv}}^t X_i^\Gamma(\tau) d\tau = 0, \\ 1, & \text{otherwise.} \end{cases} \quad (4)$$

Therefore, we can define the long-term communication service availability for the  $i$ th URLLC device in  $\Gamma$  direction as [35]

$$\alpha_i^\Gamma := \lim_{t \rightarrow \infty} \Pr \{Y_i^\Gamma(t)=1\} = \lim_{T \rightarrow \infty} \frac{1}{T} \int_0^T Y_i^\Gamma(t) dt. \quad (5)$$

The availability in  $\Gamma$  direction can be estimated over a short time period using

$$\hat{\alpha}_i^\Gamma(\Delta t_k) := \frac{1}{\Delta t_k} \int_{t_k}^{t_k+\Delta t} Y_i^\Gamma(t) dt. \quad (6)$$

In URLLC, the requirement is often defined in the form of [36]

$$\Pr \{ \alpha_i^\Gamma \leq \alpha_i^{\text{req}} \} \leq \gamma, \quad \forall i \in \mathcal{U}, \quad (7)$$

where  $\alpha_i^{\text{req}}$  is the communication service availability requirement of the use case that URLLC device  $i$  belongs to, and  $\gamma$  is the sensitivity of this use case to  $\alpha_i^{\text{req}}$ . We follow [12] in assuming that the requirement for UL and DL availability is the same for a given use case.

### B. Distributed AI Metrics: Training Delay and Accuracy

The performance of the distributed AI can be characterized by two factors: training delay (or convergence time) and training accuracy.

The convergence time of distributed AI algorithms is bounded by the communication and processing latency [7]. Let us denote the AI device selection at iteration  $k$  by an indicator vector of  $\mathcal{N}_{m,k}$  as  $\boldsymbol{\pi}_k^u = [\pi_k^u]_1, [\pi_k^u]_2, \dots, [\pi_k^u]_N$ , where  $[\pi_k^u]_i \in \{0, 1\}, \forall i \in \mathcal{N}$ . Assuming that the central node requests a subset  $\mathcal{N}_{m,k}$  (i.e.,  $\mathbf{1}^T \boldsymbol{\pi}_k^u = m_k$ ) to participate in the training while it waits for  $n (\leq m_k, \forall k \in [K])$  local gradients/models, then the AI training delay in the central node for the  $k$ th iteration,  $d_k^{\text{AI}}$ , can be derived as

$$d_k^{\text{AI}}(\boldsymbol{\pi}_k^u) := \min \left\{ \min_{\substack{\mathcal{N}_{n,k} \subseteq \mathcal{N}_{m,k}, \\ |\mathcal{N}_{n,k}|=n}} \left( \max_{i \in \mathcal{N}_{n,k}} \left( d_{i,k}^{\text{D}} + d_{i,k}^{\text{pr}} + d_{i,k}^{\text{U}} \right) \right) + d_k^{\text{pr}}, T^{\text{max}} \right\}, \quad (8)$$

where  $\boldsymbol{\pi}_k^u := [\pi_k^u]_1, \dots, [\pi_k^u]_N$  is the device selection matrix,  $d_{i,k}^{\text{D}}$ ,  $d_{i,k}^{\text{pr}}$ , and  $d_{i,k}^{\text{U}}$ , are the latency of DL transmission of the global model, local training (represented in (2b)), and UL transmission of local gradients/models for  $k$ th iteration of the  $i$ th device, respectively. It is worth noting that  $d_{i,k}^{\text{D}}$  and

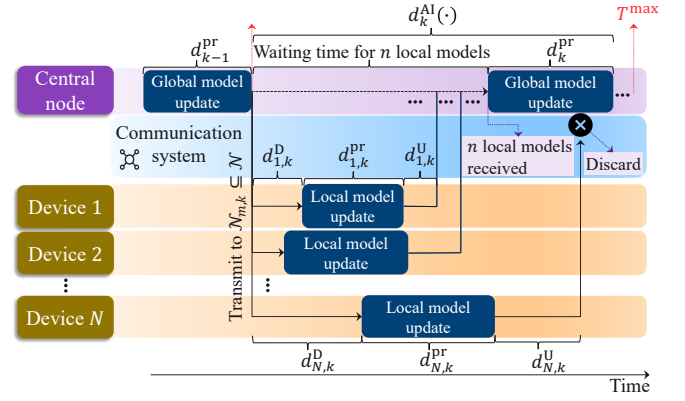


Figure 1: The illustration of training delay in distributed AI workflow.

$d_{i,k}^{\text{U}}$  include the transmission processing, payload transmission, occurred retransmissions, and queuing delay (which is determined by the number of devices sharing the same time-frequency resources in the current and previous transmission time intervals (TTIs)), and thus, are a function of  $\boldsymbol{\Pi}_k^u$ . Besides,  $d_k^{\text{pr}}$  is the  $k$ th iteration processing delay required to perform the global model update on the central node, represented in (2a). Thus, in (8), for each subset of  $\mathcal{N}_{n,k}$  with cardinality of  $n$ , the maximum aggregated communication and processing delay is calculated among devices. Then, among subsets,  $d_k^{\text{AI}}(\cdot)$  is determined by picking the subset with the lowest delay. However, to avoid an infinite waiting time in the central node, we define  $T^{\text{max}}$  as the maximum permissible delay of every iteration. Figure 1 demonstrates the training delay in  $n$ -sync distributed training.

Training accuracy is another performance metric for a distributed learning task. We can find “critical points” as the set of points where the norm of their derivative is 0. The local minima and maxima are a subset of these points. In general, under some regularity assumptions, we can often converge to an approximate critical point (a point wherein the norm of the gradients gets smaller than some positive  $\epsilon$ ). Note that a critical point may not be an optimal point, e.g., a saddle point. We denote by  $K_{\text{min}}$  the iteration number after which the algorithm converges. As we will show in Section V, our design depends on  $K_{\text{min}}$ . In the following, we provide a few examples in which we can formulate  $K_{\text{min}}$ . All examples are formally defined and presented in Appendix A-C.

**Example 1. DGD, strongly convex [25]:** Under smoothness and strong convexity assumptions of the objective functions, as well as a few more technical assumptions [25], we can show that the minimum number of iterations,  $K_{\text{min}}$ , to ensure  $\epsilon$ -accuracy<sup>2</sup> of the objective functions fulfills the following inequality:

$$K_{\text{min}} \geq \log_b \left( \frac{W^{\text{A}}}{\epsilon - \frac{z^{\text{A}}}{n}} \right) + 1, \quad (9)$$

where  $n$  is the number of participants in the global averaging step,  $W^{\text{A}}$  is a positive constant representing the initial distance to the minimal value of the global loss function,  $f(\mathbf{w}^{\star})$ , and  $z^{\text{A}}$  is a positive constant which depends on the learning

<sup>2</sup>In the case of a convex function, a critical point is the global minima.

rate, Lipschitz constant, strong convexity, and the variance of gradient noise when  $n=1$ .

**Example 2. DGD, non-convex [25]:** Under the smoothness assumption of the objective functions, we can show that the minimum number of iterations,  $K_{\min}$ , to ensure  $\epsilon$ -accuracy to a critical point, fulfills the following inequality:

$$K_{\min} \geq \frac{W^B}{\epsilon - \frac{z^B}{n}}, \quad (10)$$

where  $n$  is the number of participants in the global averaging step,  $W^B$  is a positive constant which depends on the initial distance to the lower bound of  $f$ , and  $z^B$  is a positive constant which is a function of the learning rate, Lipschitz constant, and the variance of gradient noise when  $n=1$ .

**Example 3. FL Algorithm [37]:** Consider a FL algorithm with  $E$ -step local iterations,  $N$  devices with independent and identically distributed datasets, global model averaging with  $n(\leq N)$  randomly selected local models, smooth and strongly convex objective functions. We can show that the minimum required number of iterations,  $K_{\min}$ , to ensure  $\epsilon$ -accuracy<sup>2</sup> of the objective functions would scale with

$$K_{\min} \propto \frac{1}{\epsilon} \left[ \left(1 + \frac{1}{n}\right) EG^2 + \frac{\sigma^2 + G^2}{E} + G^2 \right], \quad (11)$$

where  $G^2$  and  $\sigma^2$  are the upper bounds on the second moment of the gradient estimates and gradient noises, respectively, in different AI devices.

In (9)-(11), it is clear that the number of iterations that distributed AI requires to reach  $\epsilon$ -accuracy (i.e.,  $K_{\min}$ ) decreases as the required number of devices participating in the global update (i.e.,  $n$ ) increases in  $n$ -sync scheme. In the next section, we show how to use  $K_{\min}$  in our solution approach.

### C. Problem Formulation

Having defined the system model and the key performance indicators (KPIs) of interest, the next step is to design a device selection scheme to optimize the distributed AI training process over a wireless network, while still fulfilling the URLLC availability requirements. Then, from the definition of  $d_k^{\text{AI}}(\mathbf{\Pi}_k^u)$  in (8), the availability requirement in (7), and assuming  $n$ -sync scheme for distributed AI procedure, the joint optimization problem for distributed AI implementation over a wireless network can be expressed as follows:

$$\min_{\mathbf{\Pi}_k^u} \sum_{k=1}^K d_k^{\text{AI}}(\mathbf{\Pi}_k^u) \Omega(\mathbf{\Pi}_k^u), \quad (12)$$

$$\text{s.t. } \Pr \{ \alpha_i^\Gamma \leq \alpha_i^{\text{req}} \} \leq \gamma, \quad \forall i \in \mathcal{U}, \forall \Gamma \in \{\text{UL}, \text{DL}\}, \quad (12a)$$

$$\mathbf{1}^\top \boldsymbol{\pi}_k^u \geq n, \quad \forall k \in [K], \quad (12b)$$

$$\boldsymbol{\pi}_k^u \in \{0, 1\}^N, \quad \forall k \in [K], \quad (12c)$$

$$\Omega(\mathbf{\Pi}_k^u) \in \{0, 1\}, \quad \forall k \in [K], \quad (12d)$$

where  $\Omega(\mathbf{\Pi}_k^u)$  is a binary variable taking 1 for the iteration numbers at which the iterative algorithm has not reached  $\epsilon$ -accuracy (e.g.,  $\forall k \in [K_{\min}-1]$  for Example 1-3), and  $K$  should

be selected sufficiently large within which the distributed AI algorithm's  $\epsilon$ -accuracy is ensured. To fulfill the required number of local updates in the global update of (2) in the  $n$ -sync scheme, (12b) enforces the central node to select at least  $n$  AI devices and yet it is flexible to select any number of extra devices to tackle straggling problem (i.e.  $m_k = \mathbf{1}^\top \boldsymbol{\pi}_k^u$ , and  $m_k \in [n, n+1, \dots, N], \forall k \in [K]$ ). Moreover, (12c) indicates that device selection policy is a binary vector. Note that (12b), (12c), and (12d) must be respected at all decision time epochs.

On the one hand, the communication service availability of each URLLC device is a function of the channel state variable,  $X_i^\Gamma(t)$ , and the end-to-end delay of its packets. These two depend on many variables, such as instantaneous SINR, path gain, code rate, and transmission buffer status. On the other hand, these variables also impact the delay of the selected AI devices, influencing the training delay for each iteration. In addition, and since the URLLC service has higher priority than the distributed AI service, the amount of URLLC traffic being served on the corresponding gNB severely affects the distributed AI training delay. However, joint modeling of these URLLC and distributed AI KPIs is highly complex and mandates significant assumptions on the queue models, channel, and traffic.

## V. TRANSFORMATION TO MDP PROBLEM

The optimization problem (12) is a non-convex optimization problem. In addition, characterizing the impact of  $\boldsymbol{\pi}_k^u$  on our KPIs necessitates explicit modeling of the channel and queues, which involves approximations that may not be accurate in practice. Therefore, we propose to model the device selection problem (12) as an finite horizon MDP. Consequently, in Section V-A, we specify the state space,  $\mathcal{S}$ , action space,  $\mathcal{A}$ , and set of all possible rewards,  $\mathcal{R}$ , by dynamic interactions between the central node and RAN environment. Nevertheless, it is not possible to derive the transition probability function ( $p : \mathcal{S} \times \mathcal{R} \times \mathcal{S} \times \mathcal{A} \mapsto [0, 1]$ ) in our complex and dynamic environment. Hence, in Section V-B, we solve our device selection problem with a model-free DRL algorithm, namely SAC, to address the finite horizon fully observable discounted MDP problem.

On the path to transforming optimization problem (12) into a MDP problem, we note that our two services are on different time scales. In other words, URLLC performance should be measured based on the actual time, whilst each time step for the control loop is as long as one iteration of the distributed AI algorithm takes (i.e.,  $d_k^{\text{AI}}(\cdot)$  for  $k$ th iteration). Hence, the control loop is not periodic in actual time, and is triggered by central node. Accordingly, we use  $\Delta t_k$  (i.e.,  $t_{k+1} - t_k$ ) wherever necessary to emphasize the time instants iteration  $k$  begins and ends.

### A. MDP

The essential elements of the MDP are determined as follows.

1) *State Space,  $\mathcal{S}$* : The state space characterizes the environment. We categorize the environment's state at iteration  $k$  (i.e.,  $s_k \in \mathcal{S}$ ), into three classes i) the observations from each URLLC device, ii) the observations from each AI device, and the observations from each gNB. In the following, we describe these three classes.

**URLLC QoS variables**: Communication service availability of each URLLC device, as the main URLLC KPI, is a function of packet error ratio, mean downtime, and survival time [34], [35]. Except for survival time which is static and use case specific, the state should include both (UL/DL) packet error ratio and (UL/DL) mean downtime, estimated via empirical measurements within  $\Delta t_{k-1}$ . In addition to these measures that explicitly affect the communication service availability, cell association, (UL/DL) buffer size (at  $t_k$ ), (UL/DL) SINR, and (UL/DL) delay are other metrics that implicitly impact the availability. However, SINR and delay statistics might vary significantly during, possibly long,  $\Delta t_{k-1}$ . Hence, we represent their distribution using specific statistics of these measures, i.e., 1st percentile, 5th percentile and median of the SINR distribution, and 95th percentile, 99th percentile, and median of the delay distribution. In fact, utilizing such percentiles is well motivated by URLLC extreme availability performance, which, under proper system design, is affected by the tail of delay and SINR distributions [38].

**Distributed AI delay variables**: The training delay of each iteration,  $d_k^{\text{AI}}(\mathbf{\Pi}_k^{\text{u}})$ , is a function of the AI device selection; thus, we include a binary variable in the state indicating if this device has been selected in the last iteration. As indicated by (8), the delay of the DL transmission of the global model,  $d_{i,k}^{\text{D}}$ , and the delay of the UL transmission of local gradients/models,  $d_{i,k}^{\text{U}}$ , directly impacts the training delay, and thus, should be included in the state. Besides, (UL/DL) buffer size (at  $t_k$ ), and (UL/DL) SINR of the underlying transmissions has an implicit effect on delay, and therefore, we include them in the state. Focusing on the overall statistics (unlike URLLC service), we represent the SINR distribution of the underlying transmissions for each AI device with its 5th percentile, median and 95th percentile. Note that no empirical measurement exists for  $d_{i,k}^{\text{D}}$ ,  $d_{i,k}^{\text{U}}$ , and SINR of AI devices whose central node does not receive their local models in the  $k$ th iteration (i.e.,  $i \notin \mathcal{N}_{n,k}$ ). Moreover, if an AI device was selected at  $t_{k-1}$ , but its local update is not part of the first  $n$  received local updates, its buffer size at  $t_k$  would not be empty.

**gNB level observations**: On the gNB level, the number of resource blocks each service has consumed (in both UL and DL directions) significantly impacts both training delay and availability. Therefore, we propose to include the mean number of allocated resource blocks (per slot), within  $\Delta t_{k-1}$ , for each service in the state.

2) *Action Space,  $\mathcal{A}$* : The action space,  $\mathcal{A}$ , is the set of all possible decision variables by which the DRL agent interacts with the environment. Considering (12), our action vector at the  $k$ th iteration should be the device selection vector  $\pi_k^{\text{u}}$ . However, to mask out selections that do not follow condition (12b), we define  $\mathbf{a}_k$  as a continuous vector where each element represents the action for an AI device (i.e.,  $\mathbf{a}_k \in [-1, 1]^N$ ).

Then, the mapping from  $\mathbf{a}_k$  to  $\pi_k^{\text{u}}$  is determined by

$$\pi_k^{\text{u}} := \begin{cases} \mathbb{1}\{\mathbf{a}_k \geq \mathbf{0}\}, & \text{if } \mathbf{1}^\top \mathbb{1}\{\mathbf{a}_k \geq \mathbf{0}\} \geq n, \\ \mathbb{1}\{\mathbf{a}_k \geq a_k^{(n)} \mathbf{1}\}, & \text{otherwise,} \end{cases} \quad (13)$$

where  $a_k^{(n)}$  is the  $n$ th largest element in vector  $\mathbf{a}_k$ .

3) *The Reward Function,  $r$* : In general, the DRL agent follows an explicit goal, i.e., to maximize its cumulative discounted rewards. In other words, the reward function,  $r_{k+1}$ , is the payoff for taking action  $\mathbf{a}_k$  at state  $s_k$ . As (5) indicates, the communication service availability of URLLC devices is measured in infinite time while the temporal granularity of the DRL is determined by the amount of time each distributed AI training round takes,  $\Delta t_k$ . Therefore, we suggest using the availability estimator from Equation (6) as part of the reward function. Although estimating such a long-term measure over a short period may be imprecise, it does reflect the consequence of the device selection policy as the application layer observes it in the near future. Given the optimization objective (12) and condition (12a), we define the reward for iteration  $k+1$ ,  $r_{k+1}$ , as

$$r_{k+1} := \nu \exp \left( \zeta \min \left\{ \min_{\substack{i \in \mathcal{U}, \\ \Gamma \in \{\text{UL, DL}\}}} \left( \hat{\alpha}_i^\Gamma(\Delta t_k) - \alpha_i^{\text{req}} \right), 0 \right\} \right) + (1 - \nu) \frac{T^{\text{max}} - d_k^{\text{AI}}(\mathbf{\Pi}_k^{\text{u}})}{T^{\text{max}}}, \quad (14)$$

where  $\nu \in [0, 1]$  is the weight characterizing the relative importance between URLLC reward and distributed AI reward. In the URLLC reward,  $(\hat{\alpha}_i^\Gamma(\Delta t_k) - \alpha_i^{\text{req}})$  is negative for those URLLC devices that did not meet their corresponding availability requirement within  $\Delta t_k$ , regardless of the transmission direction,  $\Gamma$ . Hence, our reward function design enforces the DRL agent to maximize the availability of the worst URLLC device among those that do not meet their availability requirements. In addition,  $\zeta$  is a design parameter which is a function of the sensitivity ( $\gamma$ ), and the precision that the maximum availability requirement needs (i.e.,  $\zeta \propto \max_i (a_i^{\text{req}}) / \gamma$ ). Nevertheless, the device selection policy gets the full reward on the URLLC part (i.e.,  $\nu$ ) when all of the devices fulfill their availability requirements. For the distributed AI reward, the shorter  $d_k^{\text{AI}}(\cdot)$  is, the larger the  $\pi_k^{\text{u}}$ 's reward becomes. Moreover, to minimize the tail of the per-device availability distribution and the average training delay, URLLC reward decreases exponentially while the reduction in distributed AI reward is linear.

### B. Solution With Soft Actor-Critic Based Algorithm

In this paper, we employ SAC to solve the device selection MDP problem in the coexistence scenario formulated above. The following characteristics of SAC benefit our scenario [39] i) SAC is an off-policy model-free DRL algorithm in which explorations seek to find an optimal policy maximizing not only the expected accumulated discounted reward but also the expected entropy at each visited state, ii) SAC has an actor-critic architecture where the critic deep neural network (DNN) estimates state-action pair values, while the actor

DNN computes the policy, and iii) SAC conquers the massive sampling complications and minimizes the sensitivity of DRL in hyperparameters. In the rest of this section, we describe SAC in [39] for our device selection problem according to our actual implementation.

The main objective in SAC is to find an optimal stochastic policy that maximizes the discounted sum of reward and entropy. For our device selection problem, the action space  $\mathcal{A}$  has  $N$  dimensions (refer to Section V-A2). Let us denote the action space of the  $i$ th dimension, which corresponds to the action space of the  $i$ th AI device with  $\mathcal{A}_i$ . Hence, the optimal stochastic policy  $\pi^*(\cdot|s), \forall s \in \mathcal{S}$ , maps the state  $s$  to a vector of probability distributions, each over the dimension of the action space (i.e.,  $\mathcal{A}_i$ ). Thus, the objective of SAC is

$$\pi^*(\cdot|s) := \operatorname{argmax}_{\pi(\cdot|s)} \mathbb{E} \left[ \sum_{k=1}^K \lambda^{k-1} [r_{k+1} + \psi \mathbb{H}(\pi(\cdot|s_k))] \right], \quad (15)$$

where  $K, \lambda(\in [0, 1])$  and  $\psi(> 0)$  are the episode length, discount factor, and the temperature parameter specifying the relative importance between the reward and entropy terms, respectively. Furthermore,  $\mathbb{H}(\pi(\cdot|s_k)) := \mathbb{E}[-\ln(\pi(a|s_k))]$  is the entropy of policy  $\pi$  at state  $s_k$ . Introducing entropy in (15) guides the policy to explore more broadly while avoiding blatantly unfavorable trajectories.

We employ prioritized experience replay originally developed for deep Q-networks [40]. In this approach, transitions with greater temporal disparities are repeated more frequently, adding a bias toward those action. To address this issue, we remove this priority during training. Moreover, the proposed SAC-based algorithm framework makes use of target networks and clipped double Q-learning, both of which established for twin delayed deep deterministic policy gradient algorithm. According to [41], such additions can mitigate overestimation in value approximation while assuring convergence to a suboptimal policy.

The SAC algorithm (and actor-critic methods in general) uses policy iteration, in which the algorithm alternates between policy evaluation (to compute the state-action value function by  $Q_\pi(s, a)$ ) and policy improvement (to compute  $\pi$ ) in the direction of maximizing the sum of discounted return (i.e., sum of reward and a portion of entropy here). In the policy evaluation step, using the soft Bellman backup equations [39], the soft state-action value function can be computed iteratively as follows:

$$Q_\pi(s_k, a_k) = r_{k+1} + \lambda \mathbb{E}[Q(s_{k+1}, a_{k+1}) + \psi \mathbb{H}(\pi(\cdot|s_k))]. \quad (16)$$

In large-scale reinforcement learning problems where the state and action spaces are large,  $Q_\pi$  and  $\pi$  are approximated in each iteration using DNNs (via critics and actors, respectively). As mentioned before, we leverage target networks and clipped double Q-learning. Hence, in our architecture, there are 4 DNNs for the first critic, its target critic, second critic, and its target, whose weights are denoted by  $\varphi_1, \tilde{\varphi}_1, \varphi_2$ , and  $\tilde{\varphi}_2$ , respectively. In addition, there are 2 DNNs for the actor and its target network, whose weights are denoted by  $\vartheta$  and  $\tilde{\vartheta}$ , respectively. Thus,  $Q_\pi$ , in (16), is approximated by 2 DNNs as  $Q_{\varphi_i}, i \in \{1, 2\}$ .

Since it is preferable to have the offline training option, let us assume the transitions are stored in a replay buffer,  $\mathcal{B}$ . Then, regardless of sampling technique (e.g., uniform or prioritized experience replay) and the mini-batch size ( $|\mathcal{B}_{\text{mb}}|$ ), we can represent a sampled transition with  $(s, a, r, \hat{s}, I)$ , where  $I$  is a binary parameter that is 0 if the distributed AI converges in  $\hat{s}$ , and is 1, otherwise. Then,  $\varphi_1$  and  $\varphi_2$  can be trained by minimizing the mean squared error for each sampled transition as

$$J_Q(\varphi_i) := \mathbb{E} \left[ \frac{1}{2} \left( Q_{\varphi_i}(s, a) - \tilde{Q}(\hat{s}, \tilde{a}, r, I) \right)^2 \right], \quad (17)$$

where  $\tilde{a}$  is sampled from  $\pi_{\tilde{\vartheta}}(\cdot|s_{k+1})$ , and

$$\tilde{Q}(s, a, r, I) := r + I\lambda \left( \min_{i=1,2} Q_{\tilde{\varphi}_i}(s, a) - \psi \ln(\pi(a|s)) \right). \quad (18)$$

Note that the minimum represents the smallest Q-value between the two state-action value function approximations for clipped double Q-learning [41]. Then, in order to minimize  $J_Q(\cdot)$ ,  $\varphi_1$  and  $\varphi_2$  are updated in the direction of gradient descent. To ensure that temporal-difference error remains low, we update target critics' weights gradually by  $\tilde{\varphi}_i = \nu\varphi_i + (1-\nu)\tilde{\varphi}_i$  for  $i \in \{1, 2\}$  at each DRL iteration.

In the policy improvement step, the actor DNN can be updated by minimizing the expected Kullback-Leibler divergence between  $\pi_{\vartheta}$  and the exponential of the soft state-action value function, which can be rewritten as

$$J_\pi(\vartheta) := \mathbb{E} \left[ \psi \ln(\pi_{\vartheta}(a|s)) - \min_{i=1,2} Q_{\varphi_i}(s, a) \right]. \quad (19)$$

To minimize  $J_\pi(\cdot)$  based on the latest policy, we employ the re-parameterization technique, from [39], to reformulate the expectation over actions into an expectation over noise, leading to a smaller variance estimator. Therefore, we draw samples from a squashed Gaussian policy such that  $\hat{a} := \tanh(\mu_{G, \vartheta}(s) + \sigma_{G, \vartheta}(s) \cdot \chi)$ , where  $\mu_{G, \vartheta}(\cdot)$  and  $\sigma_{G, \vartheta}(\cdot)$  are the estimated mean and standard deviation of a Gaussian distribution, respectively, and  $\chi$  follows a multivariate Gaussian distribution, whose mean is a vector of 0s, and covariance matrix is the identity matrix. Hence, we can reformulate  $J_\pi(\vartheta)$  by replacing  $a$  with  $\hat{a}$  in (19). The policy parameters,  $\vartheta$ , are then updated in the gradient descent direction as in [39]. Additionally, we update the target actor weights smoothly by  $\tilde{\vartheta} = \nu\vartheta + (1-\nu)\tilde{\vartheta}$ .

Algorithm 1 summarizes the learning procedure of our SAC-based device selection solution in the coexistence scenario. Leveraging the off-policy learning capability of such an algorithm, one can train the DNNs via either the virtual network (e.g., digital twin or realistic simulations) or an operating network (e.g., in safe exploration mode). On the former,  $a_k$  can be sampled using the behavior policy in each episode, and episodes can run in parallel to speed up the training. Nevertheless, on the operating network, this algorithm can switch to on-policy learning (i.e.,  $a_k$  is sampled via the most updated policy, and episodes run consecutively). A hybrid strategy in which the DNNs are trained first with a virtual network and then tuned via an operational network could potentially result in a more efficient learning procedure.



---

**Algorithm 1: SAC-Based Algorithm for Device Selection in the Coexistence of URLLC and Distributed AI**


---

**Input:** Set of AI devices  $\mathcal{N}$ , Required number of local models in global update  $n$ ;

**Output:** Device selection policy as a function of RAN state;

**Initialize:**  $\varphi_1, \varphi_2$ , and  $\vartheta$  and set  $\tilde{\varphi}_1 \leftarrow \varphi_1, \tilde{\varphi}_2 \leftarrow \varphi_2$ , and  $\tilde{\vartheta} \leftarrow \vartheta, k \leftarrow 1$ ;

▷ **episode:** numbers of iterations during which distributed AI converges  
**foreach** *episode* **do**

    Set initial device selection, from previous virtual training or random;

**while** *true* **do**

        Receive  $c_{i,k}$  from  $n$  AI devices, or  $T^{\max}$ ;  
        Observe  $s_k$  (measured within  $\Delta t_{k-1}$ );  
        **if**  $d_k^{\text{AI}} < T^{\max}$  **then** Compute  $w_{k+1}$  as in (2a);  
        **else**  $w_{k+1} \leftarrow w_k$ ;  
        Sample an action,  $a_k \sim \pi_{\vartheta}(\cdot|s_k)$ ;  
        Transmit  $w_{k+1}$ , via RAN, to selected AI devices ( $\pi_k^u$ , derived from (13));  
        Observe  $s_{k+1}$ , and calculate  $r_{k+1}$  via (14);  
        **if** *distributed AI converges* **then**  $I_{k+1} \leftarrow 0$ ;  
        **else**  $I_{k+1} \leftarrow 1$ ;  
        Store  $(s_k, a_k, r_{k+1}, s_{k+1}, I_{k+1})$  in  $\mathcal{B}$ ;  
        **if**  $I_{k+1} = 0$  **then** break;  
         $k \leftarrow k + 1$ ;

**end**

▷ **Training DNNs**

**if**  $|\mathcal{B}| \geq |\mathcal{B}|_{\min}$  **and**  $k = l|\mathcal{B}_{\text{mb}}|, \forall l \in \{1, 2, \dots\}$  **then**

    Randomly sample a mini-batch  $\mathcal{B}_{\text{mb}}$  from  $\mathcal{B}$ ;  
    **forall**  $(s, a, r, \hat{s}, I) \in \mathcal{B}_{\text{mb}}$  **do**  
        Derive  $\hat{Q}$  using (18), where  $\tilde{a} \sim \pi_{\tilde{\vartheta}}(\cdot|\hat{s})$ ;  
    **end**  
     $\varphi_i \leftarrow \varphi_i - \frac{1}{|\mathcal{B}_{\text{mb}}|} \sum_{\forall b \in \mathcal{B}_{\text{mb}}} \hat{V} J_Q(\varphi_i)$ , for  $i \in \{1, 2\}$ ;  
     $\vartheta \leftarrow \vartheta - \frac{1}{|\mathcal{B}_{\text{mb}}|} \sum_{\forall b \in \mathcal{B}_{\text{mb}}} \hat{V} J_{\pi}(\vartheta)$ , where (19) uses  $\tilde{a}$ ;  
     $\tilde{\varphi}_i \leftarrow \nu \varphi_i + (1-\nu) \tilde{\varphi}_i$  for  $i \in \{1, 2\}$ ;  
     $\tilde{\vartheta} \leftarrow \nu \vartheta + (1-\nu) \tilde{\vartheta}$ ;

**end**

**end**

---

In the following section, we describe our simulator's modeling principles and its configuration.

## VI. SIMULATION METHODOLOGY AND CONFIGURATION

For simulating the deployment where URLLC and distributed AI services coexist, we considered a factory automation scenario, as demonstrated in Figure 2. More explicitly, we designed a 3D model of a small factory of size  $40 \times 40 \times 10 \text{ m}^3$  with 4 gNBs at the height of 8 m, and with an inter-site distance of 20 m.

### A. Channel Model

In our simulations, we considered the channel model for the indoor factory with dense clutter and high base station height

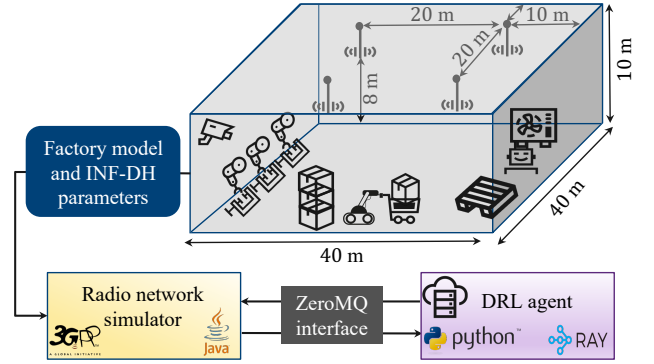


Figure 2: The simulation setup.

(InF-DH) use case, where the gNB and the devices are placed, respectively, higher and under the average height of the clutters [32]. The clutters in InF-DH use case typically represent small to medium-sized metallic machines and irregularly shaped objects. In the propagation model, the path loss is calculated by tracing the degradation in signal strength over distance under line-of-sight (LOS) and non-LOS (NLOS) circumstances. The path loss under LOS and NLOS assumptions are given by [32]

$$PL_{\text{LOS}}(d_{3\text{D}}) [\text{dB}] = 31.84 + 21.5 \log_{10}(d_{3\text{D}}) + 19 \log_{10}(f_c), \quad (20a)$$

$$PL_{\text{NLOS}}(d_{3\text{D}}) [\text{dB}] = \max(PL_{\text{LOS}}(d_{3\text{D}}), PL_{\text{DH}}(d_{3\text{D}})), \quad (20b)$$

where

$$PL_{\text{DH}}(d_{3\text{D}}) [\text{dB}] = 33.63 + 21.9 \log_{10}(d_{3\text{D}}) + 20 \log_{10}(f_c). \quad (21)$$

In above equations,  $d_{3\text{D}}$  and  $f_c$  denote the 3D distance between the device and gNB, and the center frequency, respectively. In InF-DH, the LOS probability is described by [32]

$$\text{Pr}_{\text{LOS}}(d_{2\text{D}}) = \exp\left(\frac{d_{2\text{D}} \ln(1 - r_{\text{clut}}) (h_{\text{clut}} - h_{\text{device}})}{d_{\text{clut}} (h_{\text{gNB}} - h_{\text{device}})}\right), \quad (22)$$

where  $d_{2\text{D}}$  represents the ground distance between gNB and the device. Besides,  $h_{\text{gNB}}$ ,  $h_{\text{device}}$ ,  $d_{\text{clut}}$ ,  $h_{\text{clut}}$ , and  $r_{\text{clut}}$  denote the gNB's antenna height, devices' antenna height, the typical clutter size, height and density, and are set in our simulations to 8 m, 1.5 m, 2 m, 6 m, and 60%, respectively. The shadowing for LOS and NLOS is assumed to follow a zero-mean log-normal distribution with standard deviation 4.3 and 4 in dB, respectively. In our link level simulations, we first set the position of the 4 gNBs, as shown in Figure 2. Then, for each pair of possible device positions and the 4 gNB positions, we generate uncorrelated link conditions with  $\text{Pr}_{\text{LOS}}(\cdot)$  for LOS, and  $1 - \text{Pr}_{\text{LOS}}(d_{2\text{D}})$  for NLOS. Nevertheless, the large scale parameters are generated with correlation distance of 10 m in the horizontal plane. Then, we followed the spatial consistency procedure in [32, §7.5, §7.6.3] to generate small scale parameters and channel coefficients, and used the parameters in [32, Table 7.5-6 Part-3].

### B. Radio Network Simulator and DRL Agent

The radio network simulator is event-based, 3GPP compliant, and operates at orthogonal frequency-division multiplexing (OFDM) symbol resolution. We considered numerology one from [30], implying that each slot and symbol are 0.5 ms

and  $33.33\ \mu\text{s}$  long, respectively. We assumed the channel response matrix in (3) remains constant during one slot. To ensure seamless training of distributed AI until the end of a simulation, we considered RLC in acknowledged mode for distributed AI. Nevertheless, the RLC retransmissions are slow and unlikely to benefit URLLC packets with their tight delay bounds [30]. Accordingly, we configured the RLC in unacknowledged mode for URLLC flow. Within URLLC flow, UL and DL URLLC traffic are scheduled based on round robin and delay, respectively (i.e., the packet that waited longer in the queue is scheduled first). Moreover, we used proportional-fair scheduling for distributed AI traffic in both directions. Nevertheless, we assumed strict priority scheduling where URLLC flow has higher priority than AI flow, implying that AI packets cannot be scheduled unless there is no URLLC packet in the queues.

Upon transmission, one or several packets are drawn from the head of the corresponding RLC buffer, depending on the selected modulation and coding scheme on lower layers. Alternatively, RLC could perform segmentation of packets into smaller segments to fit them into transport blocks via which the packets are transmitted. Upon reception, the received instantaneous SINR of each transport block (which depends on the radio channel and the dynamic interference of other devices' transmissions) determines an error probability. Consequently, the receptive RLC entity reassembles successfully decoded segments and delivers them to the application layer. For availability calculation on the application layer, we considered a URLLC packet lost if it is not fully received before its corresponding delay bound, followed by applying  $T_{sv}$  as in (6) where, in final availability distributions,  $\Delta t$  is the duration of one simulation, starting from the first action time (i.e.,  $t_1$ ) until  $t_K$ . Table I presents the simulation parameters.

The URLLC traffic is represented by periodic UL and DL traffic, with delay bounds of 6 ms and 4 ms as well as the sizes of 64 bytes and 80 bytes, respectively, both with a period of 6 ms. Such URLLC traffic characterization aligns with the machine control use case for mobile robots in [12]. Motivated by [42], we assumed that the shared DNN architecture (i.e., used on the devices and the central node) follows MobileNets [10], a class of efficient DNN models based on a streamlined architecture for mobile and embedded vision applications. We considered 0.25 MobileNet-224 in [10], implying that the DNN model has 0.5 million parameters. To model the distributed AI traffic, we assumed FL and 32 bits quantization for each model parameter, implying that each model (local or global) can be represented as a packet of size 2 MB. Nevertheless, our solution applies to settings where other quantization/compression approaches reduce the communication overhead [43].

In our simulation setup, the DRL agent resides in a separate server and communicates with the radio network simulator via a ZeroMQ interface. We ran the DRL agent on a server with Intel(R) Xeon(R) Gold 6132 CPU @ 2.60 GHz, 8 cores and 64 GB of RAM. In the exploration phase, we trained the DRL agent for 7 000 episodes of 50-iteration length, and our simulation time differed depending on how long each iteration (i.e.,  $d_k^{\text{AI}}(\cdot)$ ) took. Nevertheless, our SAC-based algorithm

Table I: Simulation Parameters.

Radio Network Simulator Parameters	
Parameter	Value
Deployment	4 gNBs
Duplex/Carrier frequency	FDD/2.6 GHz
gNB antenna height	8 m
Devices' height	1.5 m
Number of antenna elements in gNodeB/device	2/2
Bandwidth	40 MHz
TTI length/Subcarrier spacing	0.5 ms/30 KHz
UL/DL transmit power	0.2 W/0.5 W
Max num of UL/DL URLLC Trans. (medium access control)	3/2
Max num of UL/DL AI Trans. (medium access control)	10/10
Max num of UL/DL AI Trans. (RLC)	8/8
UL/DL URLLC delay bound	6/4 ms
UL/DL URLLC survival time, $T_{sv}$	6/6 ms
The total number of AI devices, $N$	50
The required number of local models for (2a) to progress, $n$	15
$v/\zeta$ in the reward function (14)	0.5/100
$T^{\text{max}}$	10 s
DRL Agent Parameters	
Parameter	Value
Discount factor, $\lambda$	0.1
Training mini-batch size, $ \mathcal{B}_{\text{mb}} $	200
Replay buffer size	1 000 000
Neural network hidden layers (all six)	$128 \times 128$
Prioritized replay buffer $\alpha/\beta$ in [40]	0.6/0.4
Learning rate (for critic, actor and entropy)	0.0003
$\nu$ (for smooth update)	0.002

converged with significantly fewer iterations at around 150 000 iterations. The simulation parameters are given in Table I.

In the following section, we run comprehensive simulations to study the impact of various design parameters including the distributed AI and URLLC load, the number of selected AI devices, and slicing the network resources between URLLC and distributed AI services.

## VII. RESULTS AND DISCUSSION

For the performance evaluation of our SAC-based algorithm (shown as `dRLAgent` in the figures), we set up two benchmarks.

- 1) Semi-random URLLC devices: In this benchmark, we set up 10 URLLC devices, and assume that each device moves in 1D at a speed of 30 km/h within a short distance of a position that is maintained in different simulations. Yet, the movement direction changes randomly in different seeds.
- 2) Random URLLC devices: In this benchmark, we set up 20 URLLC devices. At each simulation, the URLLC devices appear at random positions and move in 1D in a random direction at a speed of 30 km/h within a short distance of that position.

For each of these benchmarks, we compared our proposed solution with three types of baselines:

- `singleURLLC`: We did not set any distributed AI traffic in our industrial automation scenario and the URLLC devices leveraged the entire 40 MHz bandwidth.
- `mixedServ[m]`: In addition to URLLC devices, we had a total of 50 AI devices. We kept the required number of devices that the central node waits for constant (i.e.,  $n=15$ ), and randomly picked a set of  $m$

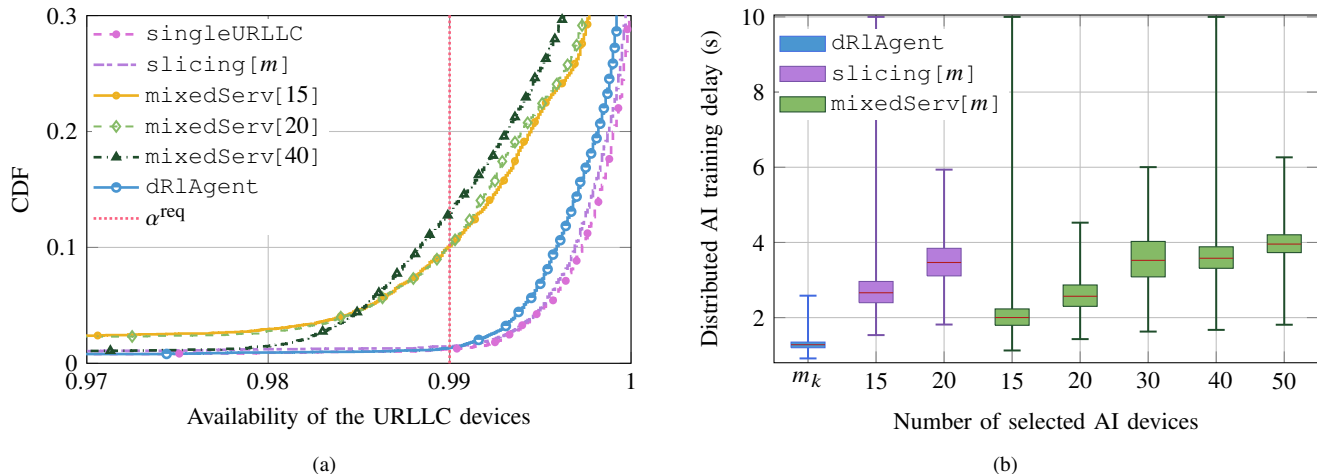


Figure 3: The empirical CDF of URLLC devices' availability,  $\hat{\alpha}_i^{\Gamma}$ , in (a), and the distributed AI training delay,  $d_k^{\text{AI}}$  in (b), both for the benchmark with semi-random URLLC devices. Each box plot represents the minimum, 25th percentile, median, 75th percentile, and maximum of the training delay distribution.

participating devices (i.e.,  $m_k = m, \forall k \in \mathbb{N}$ ), where  $m \in \{15, 20, 30, 40, 50\}$ .

- `slicing[m]`: We assigned 25% of resources to the URLLC service (i.e., 10MHz bandwidth and 0.125W for total DL transmit power), and the rest to the distributed AI service. We kept  $|\mathcal{U}|$ ,  $|\mathcal{N}|$ ,  $n$  the same as `mixedServ[m]` baseline. Besides, we randomly picked a set of  $m$  participating devices (i.e.,  $m_k = m, \forall k \in \mathbb{N}$ ), where  $m \in \{15, 20\}$ .

The `singleURLLC` baseline represents the best possible performance on the URLLC availability in our scenario. In `dRlAgent`, and to calculate the reward in (14), we set  $\nu$  and  $\zeta$  to 0.5, and 100, respectively. Besides, we assumed that all URLLC devices serve a single use case, and thus, set the availability requirement to 0.99 (i.e.,  $\alpha^{\text{req}} = \alpha_i^{\text{req}} = 0.99, \forall i \in \mathcal{U}$ ). For `singleURLLC` evaluations, we ran 102-second simulations 300 times (with different seeds). In addition, `dRlAgent`, `mixedServ[m]`, and `slicing[m]` were evaluated with 300 simulations of 50-iteration length, resulting in different simulation lengths. Note that there is no progress in distributed AI if all  $n$  local models are not collected by the central node within a time duration of  $T^{\text{max}}$ , and thus, SAC iterations could differ from distributed AI iterations. Regardless, if there is no strict latency constraint from distributed AI task, we can tune  $T^{\text{max}}$  sufficiently large to ensure that time-outs happen rarely. Although our radio network simulator can handle such situations, and for the sake of fair comparison, we set  $T^{\text{max}}=10$ s.

#### A. Semi-random URLLC Devices

Figure 3 shows the distribution of our main KPIs. Figure 3a illustrates the empirical cumulative density function (CDF) of URLLC devices' availability, where each sample is the UL or DL availability of one URLLC device in one simulation during its whole simulation time. In `slicing[m]`, due to slicing of the bandwidth and gNB transmission power, the availability distribution is identical for any arbitrary  $m$ . As this figure shows, compared to `singleURLLC` and

`slicing[m]`, the availability of the URLLC devices decreases in `mixedServ[15]` and `mixedServ[20]`, likely, because of the introduced interference by AI devices in the neighboring cells. Although the scheduler adjusts the modulation and coding scheme to deal with this additional interference<sup>3</sup>, it still affects the availability, such that the availability requirement of 0.99 can be met with sensitivity of around 0.1 in `mixedServ[15]` and `mixedServ[20]`, rather than 0.012 in `singleURLLC` and 0.014 in `slicing[m]` (see (7)). In `mixedServ[m]` baselines, most of the availability samples are still greater than or equal to 0.98. Unlike many conventional services, such decrease is not acceptable for URLLC service. Despite the impact of introducing the large load of the distributed AI service, we observe that our `dRlAgent` solution keeps the URLLC devices' availability close to the `singleURLLC` and `slicing[m]` up to  $\alpha^{\text{req}}$ , and can support the availability requirement of 0.99 with sensitivity of 0.013.

Figure 3b depicts the distributed AI training delay. Each box shows the minimum, 25th percentile, median, 75th percentile, and the maximum of the observed training delay samples. In general, as `slicing[m]` and `mixedServ[m]` boxes, and our results in [9] suggest, the training delay grows as the number of selected devices increases. However, it is more likely for central node to wait excessively for stragglers, and thus reach time-out when  $m=n$  (i.e., in both `slicing[15]` and `mixedServ[15]`). Moreover, the lower training delay statistics in `mixedServ[15]` and `mixedServ[20]` than `slicing[15]` and `slicing[20]`, respectively, suggests that distributed AI service in `mixedServ[m]` generally consumes more resources than the allocated resources in `slicing[m]`. As this figure indicates, compared to the most competitive baseline (i.e., `mixedServ[15]`), our `dRlAgent` decreases the median training delay by 36%, while the maximum observed training delay is 2.6s, i.e., 43% less than

<sup>3</sup>Note that such decrease in availability occurs regardless of the scheduler configuration. For example, higher target block error rate cannot overcome the extra interference, and lower target block error rate leads to extra delay, both resulting in lower availability.

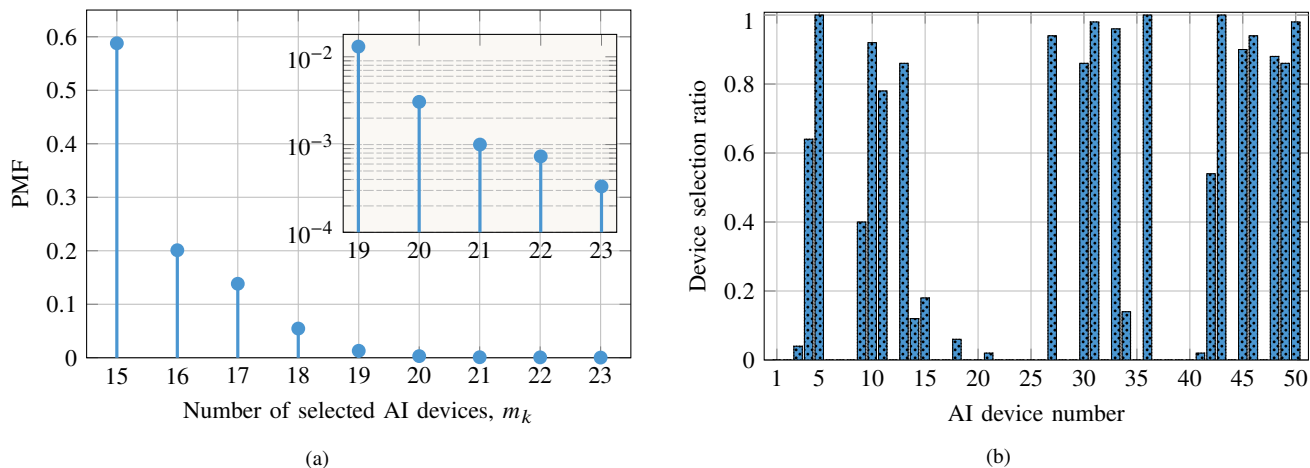


Figure 4: The empirical probability mass function of the number of (a) selected devices, and (b) AI device participation ratio, both for dRlAgent.

mixedServ[20], which has the lowest maximum observed training delay among the baselines.

Figure 4 demonstrates the device selection policy in the evaluation phase,  $\pi_k^u$ , for dRlAgent. Figure 4a shows the empirical probability mass function (PMF) of the number of selected AI devices,  $m$  for different iterations. As this figure indicates, given that we set  $n=15$  in all of our evaluations, our SAC-based solution selected at least 1 extra AI device for more than 40% of iterations. Such selection of extra devices implies that our device selection solution could still leverage the diversity introduced by extra AI devices, even in our bandwidth-limited deployment. Carefully selected extra devices reduce the sensitivity to the straggler problem and therefore reduce the overall latency without substantial impact on the interference footprint. Figure 4b represents the device selection ratio for each AI device that is the number of times an AI device is selected by the DRL agent divided by the total number of iterations in the evaluation phase. According to Figure 4b, 9 AI devices are selected in more than 90% of the iterations. Also, 24% of the AI devices are selected with a ratio of 0.1 to 0.9.

### B. Random URLLC Devices

Figure 5 illustrates the distribution of availability for URLLC devices (in Figure 5a) and training delay of distributed AI service (in Figure 5b). As Figure 5a shows, up to  $\alpha^{\text{req}}$ , dRlAgent keeps the availability of AI devices close to singleURLLC, even though the URLLC traffic appears at random locations in different seeds. Surprisingly, slicing[ $m$ ] can support 0.99 availability requirement with  $\gamma=0.02$ , which is more than twice the sensitivity singleURLLC and dRlAgent can support. Compared to the semi-random benchmark, in this benchmark, the number of URLLC devices is doubled and they can appear in any part of the factory. Hence, slicing[ $m$ ] might associate a large number of devices to the same gNB, contributing to lower availability performance with 10 MHz bandwidth and 0.125 W maximum DL transmission power for URLLC devices. In Figure 5b, as expected, the delay distribution of slicing[ $m$ ], for  $m \in \{10, 15\}$ , does not show any significant

difference with Figure 3b, and we observe a slight raise in overall training delay distribution of mixedServ[ $m$ ] for  $m \in \{10, 15\}$  (in the order of tens of milliseconds). Nevertheless, our dRlAgent improves the median training delay at least by 30% (compared to mixedServ[15]), and decreases the maximum observed training delay at least by 15% (compared to mixedServ[20]). Therefore, even in fully-random URLLC devices benchmark, our dRlAgent successfully orchestrates the distributed AI traffic such that i) the impact on the availability of the URLLC devices, given their requirement, is negligible, and ii) it reaches lower training delay statistics.

## VIII. CONCLUSIONS

In this paper, we investigated the performance optimization of distributed AI when it coexists with the URLLC service with stringent operational requirements. We proposed a DRL-powered framework to run distributed AI using a carefully selected subset of devices with the objective of minimizing the AI training delay while maintaining the URLLC communication service availability requirements. Our comprehensive 3GPP-compliant 5G simulations indicate that our scheme can significantly decrease the total training delay while keeping URLLC devices' availability near the single service scenario (i.e., when all network resources are allocated to the URLLC devices). This paper provides useful insights on how to adaptively control AI traffic (via device selection) to ensure a sustainable coexistence between distributed AI and URLLC.

An alternative approach to control the load of distributed AI is through quantization of the exchanged messages. These approaches often reduce the communication overhead per iteration (and thereby interference footprint) at the expense of some extra iterations to reach convergence. Potential future work is to develop novel approaches that adaptively change the quantization level based on not only the distributed AI algorithm but also the load of the URLLC and the interference footprint of the network.

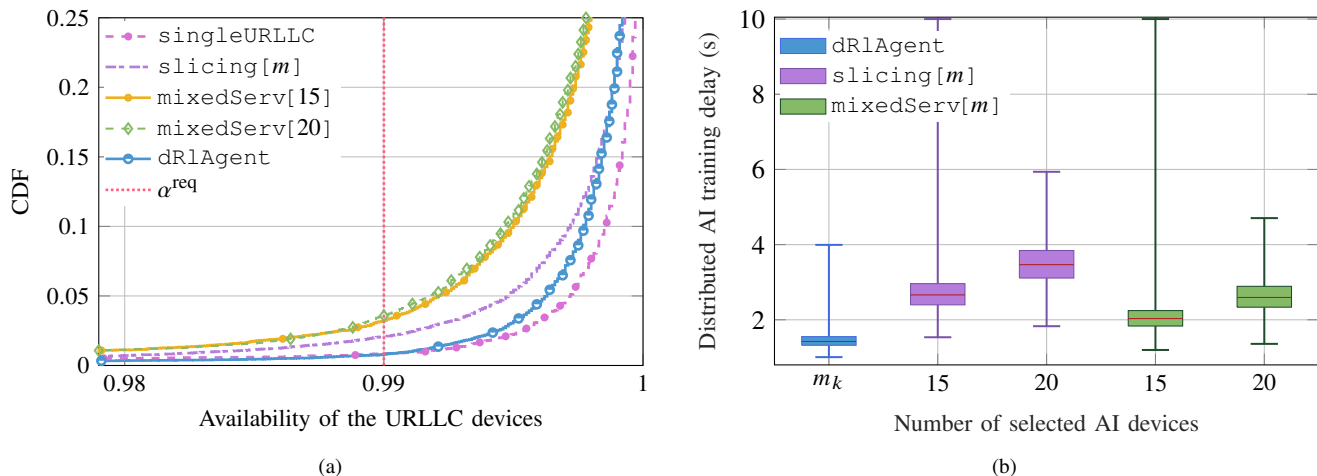


Figure 5: The empirical CDF of URLLC devices' availability,  $\alpha_i^F$ , in (a), and the distributed AI training delay,  $d_k^{\text{AI}}$  in (b), both for the benchmark with random URLLC devices. Each box plot represents the minimum, 25th percentile, median, 75th percentile, and maximum of the observed training delay samples.

#### APPENDIX A EXAMPLE 1 SHOW CASE

Towards solving the distributed optimization problem (1), the central node performs the gradient descent update at each iteration  $k$  as

$$\mathbf{w}_{k+1} = \mathbf{w}_k - \frac{\eta_k}{n} \sum_{i \in \mathcal{N}_{n,k}} \widehat{\nabla} f_i(\mathbf{w}_k), \quad (23)$$

where the right hand side of the equation represents  $A(\cdot)$  in (2a),  $\widehat{\nabla} f_i(\mathbf{w}_k)$  is the true gradient's noisy estimation at the  $i$ th AI device, and  $\mathcal{N}_{n,k}$  is the set of AI devices from which central node received the first  $n$  local updates at the  $k$ th iteration. We assume that each AI device employs mini-batch gradient descent, and to simplify our notation, the size of the mini-batches are assumed the same for all devices in all iterations. Hence, the overall gradient estimate using the local estimates of the AI devices can be obtained as

$$\frac{1}{n} \sum_{i \in \mathcal{N}_{n,k}} \widehat{\nabla} f_i(\mathbf{w}_k) := \nabla f(\mathbf{w}_k) + \bar{\mathbf{e}}_k^{(n)}, \quad (24)$$

where  $\bar{\mathbf{e}}_k^{(n)} := \frac{1}{n} \sum_{i \in \mathcal{N}_{n,k}} \mathbf{e}_{i,k}$ , and  $\mathbf{e}_{i,k}$  is the residual term of the  $i$ th device's estimate at the  $k$ th iteration, while  $\nabla f(\mathbf{w}_k)$  is the true gradient (i.e., the gradient of the batch gradient descent on centralized training). Let us make the following assumptions.

**Assumption 1.** [25], [37] The objective functions  $f_i$ ,  $\forall i \in \mathcal{N}$ , are all  $L$ -smooth, with Lipschitz constant  $L > 0$ .

**Assumption 2.** [25], [37] The objective functions  $f_i$ ,  $\forall i \in \mathcal{N}$ , are all strongly convex, with constant  $\mu > 0$ .

**Assumption 3.** [25] There exist  $\beta_2 \geq (\beta_1 + 1)^2 > 0$  that, for  $\forall k \in [K]$  and  $\forall i \in \mathcal{N}$ , the objective function  $f(\mathbf{w})$  and the DGD algorithm have the following limits:

$$\nabla f(\mathbf{w}_k)^\top \mathbb{E}[\mathbf{e}_{i,k}] \geq \beta_1 \|\nabla f(\mathbf{w}_k)\|_2^2, \quad (25a)$$

$$\nabla f(\mathbf{w}_k)^\top \mathbb{E}[\mathbf{e}_{i,k}] \leq \beta_2 \|\nabla f(\mathbf{w}_k)\|_2^2. \quad (25b)$$

It is worth mentioning that (25a) implies that the noisy estimation of the gradient is on the same half space with

the true gradient, and (25b) is a weaker assumption of the bounded variance of  $\sum_{i \in \mathcal{N}_{n,k}} \widehat{\nabla} f_i(\mathbf{w}_k)/n$ , and only bounds it by the actual gradient,  $\nabla f(\mathbf{w}_k)$ .

**Assumption 4.** [25], [37] The variance of the gradient norms in each device is bounded, i.e.,

$$\mathbb{E}[\|\mathbf{e}_{i,k}\|_2^2] \leq \sigma^2, \forall k \in [K], \forall i \in \mathcal{N}. \quad (26)$$

Since,  $\bar{\mathbf{e}}_k^{(n)}$  is an unbiased estimator of  $\mathbb{E}[\mathbf{e}_{i,k}]$ , we have

$$\mathbb{E}[\|\bar{\mathbf{e}}_k^{(n)}\|_2^2] \leq \frac{\sigma^2}{n}, \forall k \in [K]. \quad (27)$$

It is worth noting that (25b) and (26) results in

$$\mathbb{E}[\|\widehat{\nabla} f_i(\mathbf{w}_k)\|_2^2] \leq \sigma^2 + \beta_2 \|\nabla f(\mathbf{w}_k)\|_2^2. \quad (28)$$

Then, if Assumptions 1-4 hold, for a fixed learning rate  $\eta$  that is  $0 < \eta \leq \frac{\beta_1 + 1}{(2\beta_2 + 1)L}$ , we have [25, Theorem 4.6]

$$\mathbb{E}[f(\mathbf{w}_k) - f(\mathbf{w}^*)] \leq \frac{\eta L \sigma^2}{2n\beta_1\mu} + (1 - \eta\beta_1\mu)^{k-1} \left( f(\mathbf{w}_1) - f(\mathbf{w}^*) - \frac{\eta L \sigma^2}{2n\beta_1\mu} \right), \quad (29)$$

where the first term represents the gap to the expected optimal value that DGD converges to when  $k \rightarrow \infty$  for a fixed learning rate, and the second term is the convergence rate. Using the learning rate bound and Assumption 3, and the fact that  $\mu \leq L$  (as a result of Assumption 1 and 2), we can derive that  $\eta\beta_1\mu < 1$ , and hence,  $(1 - \eta\beta_1\mu)$  is a contraction factor.

Let us assume that our initial point is within a bounded region with respect to the final point that we can converge (i.e., the last parenthesis in (29) is less than or equal to  $W^A$ ). Note that the additional term of  $\eta L \sigma^2 / 2n\beta_1\mu$  reflects that DGD cannot converge to the optimal value, but instead, to a neighborhood of  $f(\mathbf{w}^*)$ . Then, the minimum required number

of iterations,  $K_{\min}$ , to reach  $\epsilon$ -accuracy becomes

$$K_{\min} \geq \log_{(1-\eta\beta_1\mu)} \left( \epsilon - \frac{\eta L \sigma^2}{2n\beta_1\mu} \right) - \log_{(1-\eta\beta_1\mu)}(W) + 1. \quad (30)$$

Then, (30) can be simplified as

$$K_{\min} \geq \log_b \left( \frac{W^A}{\epsilon - \frac{z^A}{n}} \right) + 1, \quad (31)$$

where  $b := 1/(1-\eta\beta_1\mu) > 1$ , and  $z^A$  is a positive constant which depends on the learning rate, Lipschitz constant, strong convexity, and the error in the gradient estimates for  $n=1$ .

#### APPENDIX B EXAMPLE 2 SHOW CASE

**Assumption 5.** [25] The objective functions  $f_i$ ,  $\forall i \in \mathcal{N}$ , are lower bounded by a scalar  $f_{\inf}$  for all sequences of  $\mathbf{w}_k$ .

The non-convex objective functions may contain several local minima and other stationary points. Therefore, we define the convergence criteria on the gradient. Then, if Assumptions 1, 3-5 hold, for a fixed learning rate satisfying  $0 < \eta \leq \frac{\beta_1+1}{L(2\beta_2+1)}$ , we have [25, Theorem 4.8]

$$\mathbb{E} \left[ \frac{1}{K} \sum_{k=1}^K \|\nabla f(\mathbf{w}_k)\|_2^2 \right] \leq \frac{\eta L \sigma^2}{n(\beta_1+1)} + \frac{2(f(\mathbf{w}_1) - f_{\inf})}{\eta(\beta_1+1)K}. \quad (32)$$

To understand (32), consider centralized training and batch gradient descent, where there exist no gradient noise, and  $\sigma^2$  becomes zero, resulting in  $\|\nabla f(\mathbf{w}_k)\|_2 \rightarrow 0$  as  $K$  enlarges. However, in DGD, the average norm of gradients converges to  $\eta L \sigma^2 / n(\beta_1+1)$ . Now, the required number of iterations,  $K_{\min}$ , to reach  $\epsilon$ -accuracy becomes

$$K_{\min} \geq \frac{2(f(\mathbf{w}_1) - f_{\inf})}{\eta(\beta_1+1) \left( \epsilon - \frac{\eta L \sigma^2}{n(\beta_1+1)} \right)}. \quad (33)$$

In (33), we observe that loosening the convergence criteria (i.e., as  $\epsilon$  increases) leads to a higher required number of iterations to reach  $\epsilon$ -accuracy. We can simplify (33) as

$$K_{\min} \geq \frac{W^B}{\epsilon - \frac{z^B}{n}}, \quad (34)$$

where  $W^B := 2(f(\mathbf{w}_1) - f_{\inf}) / \eta(\beta_1+1)$ , and  $z^B$  is a function of the learning rate, Lipschitz constant, and error in the gradient estimates when  $n=1$ . Note that  $\epsilon$  should be set to a value that is larger than the neighborhood DGD can potentially converge to (i.e.,  $z^B$ ).

#### APPENDIX C EXAMPLE 3 SHOW CASE

There are two main differences between FL and DGD, i) there could be several local iterations in each AI device between two communications, and ii) the model parameters (i.e., the weights of the DNNs) are communicated, rather than the gradients in DGD. Hence, on the local update, each AI device performs (23) for  $E$  times before updating the global iteration  $k$ , as (2b).

**Assumption 6.** [37] The variance of the gradient estimates in each AI device is bounded, i.e.,

$$\mathbb{E} \left[ \left\| \widehat{\nabla} f_i(\mathbf{w}_k) \right\|_2^2 \right] \leq G^2. \quad (35)$$

Note that (35) is a stricter assumption than Assumptions 3 and 4, combined, as shown in (28).

If Assumptions 1, 2, 4, and 6 hold, and  $n$  AI devices are selected uniformly at each iteration, then for a diminishing learning rate  $\eta_k = 2/\mu(\xi + k + \kappa)$ , where  $\kappa \in [E-1]$  is the local iteration number and  $\xi := \max\{8L/\mu, E\}$ , the following inequality holds [37, Theorem 3]:

$$\mathbb{E}[f(\mathbf{w}_k) - f(\mathbf{w}^*)] \leq \frac{2L \left( \frac{\sigma^2}{N} + 8(E-1)^2 + \rho E^2 G^2 + \xi G^2 \right)}{\mu^2(\xi + k + \kappa - 1)}, \quad (36)$$

where  $\rho := \frac{4(N-n)}{n(N-1)}$ . Hence, the minimum number of global iterations (i.e., rounds of communications) to attain  $\epsilon$ -accuracy approximately becomes [37]

$$K_{\min} \propto \frac{1}{\epsilon} \left[ \left( 1 + \frac{1}{n} \right) E G^2 + \frac{\frac{\sigma^2}{N} + G^2}{E} + G^2 \right], \quad (37)$$

where we assumed  $\xi = O(1 + E)$ .

#### REFERENCES

- [1] Y. Shi, K. Yang, T. Jiang, J. Zhang, and K. B. Letaief, "Communication-efficient edge AI: Algorithms and systems," *IEEE Commun. Surveys Tuts.*, vol. 22, no. 4, pp. 2167–2191, 2020.
- [2] H. Huang *et al.*, "Real-time fault detection for IIoT facilities using GBRBM-based DNN," *IEEE Internet Things J.*, vol. 7, no. 7, pp. 5713–5722, 2020.
- [3] T. Li, A. K. Sahu, A. Talwalkar, and V. Smith, "Federated learning: Challenges, methods, and future directions," *IEEE Signal Process. Mag.*, vol. 37, no. 3, pp. 50–60, 2020.
- [4] A. Alabbasi, M. Ganjalizadeh, K. Vandikas, and M. Petrova, "On cascaded federated learning for multi-tier predictive models," in *IEEE Int. Conf. on Commun. Workshops (ICC Workshops)*, 2021.
- [5] S. Dutta, G. Joshi, S. Ghosh, P. Dube, and P. Nagpurkar, "Slow and stale gradients can win the race: Error-runtime trade-offs in distributed SGD," in *Proc. 21st Int. Conf. Artif. Intell. Stat. (AISTATS)*, 2018.
- [6] B. McMahan, E. Moore, D. Ramage, S. Hampson, and B. A. y. Arcas, "Communication-efficient learning of deep networks from decentralized data," in *Proc. 20th Int. Conf. Artif. Intell. Stat. (AISTATS)*, 2017.
- [7] M. Chen, H. V. Poor, W. Saad, and S. Cui, "Convergence time optimization for federated learning over wireless networks," *IEEE Trans. Wireless Commun.*, vol. 20, no. 4, pp. 2457–2471, 2021.
- [8] M. Chen *et al.*, "Distributed learning in wireless networks: Recent progress and future challenges," *IEEE J. Sel. Areas Commun.*, 2021.
- [9] M. Ganjalizadeh, H. S. Ghadikolaei, J. Haraldson, and M. Petrova, "Interplay between distributed AI workflow and URLLC," 2022, *arXiv:2208.01352* [cs.NI].
- [10] A. G. Howard *et al.*, "MobileNets: Efficient convolutional neural networks for mobile vision applications," 2017, *arXiv:1704.04861* [cs.CV].
- [11] S. Wan, J. Lu, P. Fan, Y. Shao, C. Peng, and K. B. Letaief, "Convergence analysis and system design for federated learning over wireless networks," *IEEE J. Sel. Areas Commun.*, vol. 39, no. 12, pp. 3622–3639, 2021.
- [12] *Service requirements for cyber-physical control applications in vertical domains*, 3GPP, TS 22.104 v18.0.0, 2021.
- [13] *Service requirements for the 5G system*, 3GPP, TS 22.261 v18.6.1, 2022.
- [14] J. Sachs, G. Wikstrom, T. Dudda, R. Baldemair, and K. Kittichokechai, "5G radio network design for ultra-reliable low-latency communication," *IEEE Netw.*, vol. 32, no. 2, pp. 24–31, 2018.
- [15] A. K. Bairagi *et al.*, "Coexistence mechanism between eMBB and uRLLC in 5G wireless networks," *IEEE Trans. Commun.*, vol. 69, no. 3, pp. 1736–1749, 2021.

- [16] A. Anand, G. De Veciana, and S. Shakkottai, "Joint scheduling of URLLC and eMBB traffic in 5G wireless networks," *IEEE/ACM Trans. Netw.*, vol. 28, no. 2, pp. 477–490, 2020.
- [17] S. R. Sabuj, A. Ahmed, Y. Cho, K.-J. Lee, and H.-S. Jo, "Cognitive UAV-aided URLLC and mMTC services: Analyzing energy efficiency and latency," *IEEE Access*, vol. 9, pp. 5011–5027, 2021.
- [18] P. Popovski, K. F. Trillingsgaard, O. Simeone, and G. Durisi, "5G wireless network slicing for eMBB, URLLC, and mMTC: A communication-theoretic view," *IEEE Access*, vol. 6, pp. 55 765–55 779, 2018.
- [19] M. M. Amiri, D. Gündüz, S. R. Kulkarni, and H. V. Poor, "Convergence of update aware device scheduling for federated learning at the wireless edge," *IEEE Trans. Wireless Commun.*, vol. 20, no. 6, pp. 3643–3658, 2021.
- [20] S. Samarakoon, M. Bennis, W. Saad, and M. Debbah, "Distributed federated learning for ultra-reliable low-latency vehicular communications," *IEEE Trans. Commun.*, vol. 68, no. 2, pp. 1146–1159, 2020.
- [21] K. Wei *et al.*, "Low-latency federated learning over wireless channels with differential privacy," *IEEE J. Sel. Areas Commun.*, vol. 40, no. 1, pp. 290–307, 2022.
- [22] W. Zhang *et al.*, "Optimizing federated learning in distributed industrial IoT: A multi-agent approach," *IEEE J. Sel. Areas Commun.*, vol. 39, no. 12, pp. 3688–3703, 2021.
- [23] M. Chen, Z. Yang, W. Saad, C. Yin, H. V. Poor, and S. Cui, "A joint learning and communications framework for federated learning over wireless networks," *IEEE Trans. Wireless Commun.*, vol. 20, no. 1, pp. 269–283, 2021.
- [24] C. T. Dinh *et al.*, "Federated learning over wireless networks: Convergence analysis and resource allocation," *IEEE/ACM Trans. Netw.*, vol. 29, no. 1, pp. 398–409, 2021.
- [25] L. Bottou, F. Curtis, and J. Nocedal, "Optimization methods for large-scale machine learning," *SIAM Review*, vol. 60, no. 2, pp. 223–311, 2018.
- [26] K. Scaman, F. Bach, S. Bubeck, L. Massoulié, and Y. T. Lee, "Optimal algorithms for non-smooth distributed optimization in networks," *Adv. Neural Inf. Process. Syst. (NeurIPS)*, vol. 31, 2018.
- [27] H. S. Ghadikolaei, S. Stich, and M. Jaggi, "LENA: Communication-efficient distributed learning with self-triggered gradient uploads," in *Proc. 24th Int. Conf. Artif. Intell. Stat. (AISTATS)*, 2021.
- [28] S. Ji, W. Jiang, A. Walid, and X. Li, "Dynamic sampling and selective masking for communication-efficient federated learning," *IEEE Intell. Syst.*, vol. 37, no. 2, pp. 27–34, 2022.
- [29] T. Chen, G. Giannakis, T. Sun, and W. Yin, "LAG: Lazily aggregated gradient for communication-efficient distributed learning," in *Adv. Neural Inf. Process. Syst. (NeurIPS)*, 2018.
- [30] E. Dahlman, S. Parkvall, and J. Skold, *5G NR: The next generation wireless access technology*. Academic Press, 2018.
- [31] M. Cohen, J. Diakonikolas, and L. Orecchia, "On acceleration with noise-corrupted gradients," in *Proc. Int. Conf. Mach. Learn. (ICML)*, 2018.
- [32] *Study on channel model for frequencies from 0.5 to 100 GHz*, 3GPP, TR 38.901 v17.0.0, 2022.
- [33] "Service-level specifications (SLSS) for 5G technology-enabled connected industries," 5G Alliance for Connected Industries and Automation (5G-ACIA), Frankfurt, Germany, White Paper, 2021. [Online]. Available: <https://5g-acia.org/whitepapers/service-level-specifications-slss-for-5g-technology-enabled-connected-industries/>
- [34] M. Ganjalizadeh, A. Alabbasi, J. Sachs, and M. Petrova, "Translating cyber-physical control application requirements to network level parameters," in *IEEE 31st Annu. Int. Symp. Pers. Indoor Mob. Radio Commun. (PIMRC)*, 2020.
- [35] M. Ganjalizadeh, A. Alabbasi, A. Azari, H. S. Ghadikolaei, and M. Petrova, "An RL-based joint diversity and power control optimization for reliable factory automation," in *IEEE Glob. Commun. Conf. (GLOBECOM)*, 2021.
- [36] P. Popovski *et al.*, "Wireless access in ultra-reliable low-latency communication (URLLC)," *IEEE Trans. Commun.*, vol. 67, no. 8, pp. 5783–5801, 2019.
- [37] X. Li, K. Huang, W. Yang, S. Wang, and Z. Zhang, "On the convergence of FedAvg on non-IID data," in *Int. Conf. on Learn. Represent. (ICLR)*, 2020.
- [38] M. Bennis, M. Debbah, and H. V. Poor, "Ultrareliable and low-latency wireless communication: Tail, risk, and scale," *Proc. of the IEEE*, vol. 106, no. 10, pp. 1834–1853, Oct. 2018.
- [39] T. Haarnoja *et al.*, "Soft actor-critic algorithms and applications," 2018, *arXiv:1812.05905* [cs.LG].
- [40] T. Schaul, J. Quan, I. Antonoglou, and D. Silver, "Prioritized experience replay," in *Int. Conf. on Learn. Represent. (ICLR)*, 2016.
- [41] S. Fujimoto, H. van Hoof, and D. Meger, "Addressing function approximation error in actor-critic methods," in *Proc. Int. Conf. Mach. Learn. (ICML)*, 2018.
- [42] *5G System (5GS); Study on traffic characteristics and performance requirements for AI/ML model transfer*, 3GPP, TR 22.874 v18.2.0, 2021.
- [43] S. Magnusson, H. S. Ghadikolaei, and N. Li, "On maintaining linear convergence of distributed learning and optimization under limited communication," *IEEE Trans. Signal Process.*, vol. 68, pp. 6101–6116, 2020.